UCRL-JC-125391
PREPRINT

Foam and Structural Response Calculations for NIF Neutron Exposure Sample Case Assembly Design

G. DiPeso
F. Serduke
L. Pittenger

This paper was prepared for submittal to the
Nuclear Explosives Code Developers Conference
San Diego, CA
October 22-25, 1996

October 17, 1996

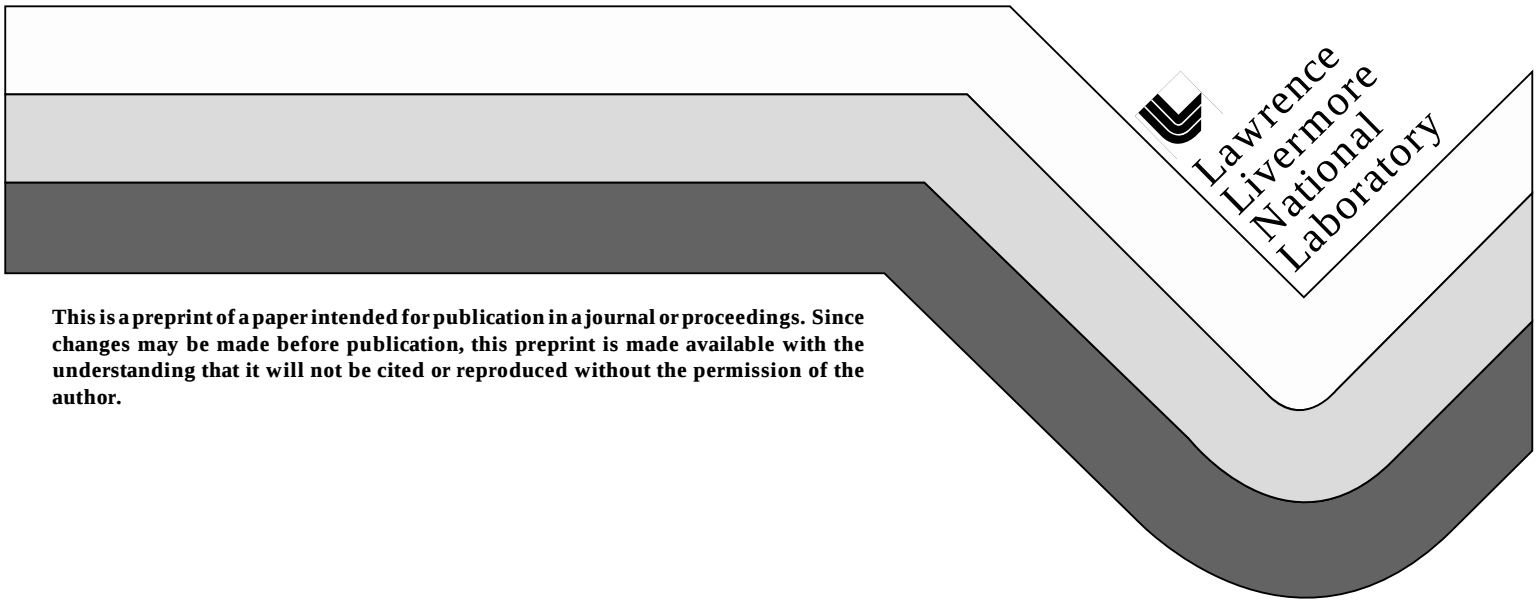

Foam and Structural Response Calculations for NIF Neutron Exposure Sample Case Assembly Design (U)

Gregory DiPeso, Frank Serduke, and Lee Pittenger
Lawrence Livermore National Laboratory

We describe the calculations used to design an aluminum foam protection layer for a stainless steel neutron exposure sample case. The layer protects the case from impulsive loads generated by a 20 MJ NIF capsule 10 cm from the sample case assembly. Impulse only from ablating x-rays and hohlraum plasma debris is considered. One dimensional CALE foam response calculations and analytic estimates are used to show that 1 cm of aluminum 6101-T6 foam 10 % of solid density is sufficient to attenuate the incoming peak pressure without complete melting on crush-up. Two dimensional DYNA calculations show that a 304 stainless steel spherical shell sample case with an inner radius of 1 cm and a wall thickness of 2 mm encased in 1 cm of foam does not yield to the pressure that is transmitted through the foam by a 220 Pa-sec (2.2 ktap), 2 GPa (20 kbar) load due to recoil of x-ray ablation. An unprotected spherical shell case subjected to a gentler load with peak pressure reduced to 0.2 GPa (2 kbar) not only yields but its effective plastic strain exceeds the failure point of 0.4 in 304 stainless steel after 160 μsec. Doubling the impulse for the protected case to approximately account for debris loading results in very localized yield and an effective plastic strain that does not exceed 0.014. (U)

1.0 Introduction

The purpose of this report is to summarize the calculations done for designing NIF sample case assemblies. The simplest sample case assembly for neutron exposure is a metal case surrounded by a shock absorbing foam. The foam is metal based since polymer foams could lose their strength due to neutron and x-ray heating and ceramic foams crumble during crush-up. The foam surface is covered with a 1 mm of ice or some other ablating material that is innocuous to target chamber parts and cryogenics, i.e. does not coat optical surfaces. This thin layer is needed so that the foam itself is not ablated. Calculations presented here will show foam shock attenuation performance and assembly structural response for a preliminary design.

The ice/foam concept proposed by Kruger [1] is a method by which NIF target chamber parts (e.g. target positioner, sample cases) can be protected from an impulse load due to cold (100 eV BB) x-rays and plasma debris generated by a disassembling hohlraum. The ice guarantees absorption of the cold x-rays but the resulting ablation contributes to recoil impulse. For a 20 MJ capsule 10 cm away from the front face of an ice/foam layer, the cold x-ray portion of the impulse has been simulated with the result that as the recoil pressure pulse progresses to 1 mm depth in the ice, the peak pressure is 1.8 GPa (18 kbar) and the impulse is 220 Pa-sec (2.2 ktap) [2]. The plasma debris portion of the impulse is a subject of ongoing simulations. Managan's calculations show an additional 150 Pa-sec (1.5 ktap) impulse due to a 30 micron hohlraum [3]. Also, Per Peterson of the UC Berkeley Nuclear Engineering Department showed that for a combination of hohlraum cold x-rays and debris plasma impinging on a frost layer, the peak pressure stays around 2 GPa but the impulse is slightly more than doubled [4]. We use these numbers as a starting point to calculate the foam thickness required to attenuate the pulse.

Since momentum is conserved, the sharp pressure pulse is attenuated into a much weaker but much longer pulse. The material response to the long time pulse dictates the design of the sample case that is surrounded by the foam, particularly the case wall thickness. We chose stainless steel as a material since our NIF neutron exposure tests will include liquids. Rounded corners are a simple way to reduce stress concentrations and taking this idea as far as it can go, we chose a spherical shell case shape. The final design will probably look more like a test tube with some mechanism to seal the top. The structural response of the final design as well as protection mechanisms for macroscopic debris in the target chamber, e.g. cryo tube shrapnel, are not considered in this report.

The report is divided into four more sections. Section 2 is a detailed discussion of foam dynamics. Section 3 gives CALE [5] calculations of foam performance with comparisons to the analytical model of Section 2. Section 4 gives DYNA [6] structural

response calculations of the sample case assembly and a bare sample case to demonstrate the necessity of the foam. Section 5 describes future work.

2.0 Foam dynamics

A generic stress strain curve for a foam is shown in Fig. 1. According to Gibson-Ashby [7], the plateau or foam yield stress for plastic failure of foam cell joints is given by

$$\sigma_p = a\sigma_{ys}\delta^{3/2} \quad (1)$$

where δ is the ratio of the initial foam density to the base material density, σ_{ys} is the base material yield strength and a is a fitting constant. A good foam to consider for our purposes is ERG's Duocel foam, based on aluminum alloy 6101-T6 [8]. All subsequent appearance of aluminum in this report should be understood to mean this particular alloy. The alloy has a density of 2700 kg/m^3 and a yield strength of about 195 MPa over a range of -80 to 20 C [9]. Given initial NIF cryo conditions and neutron and x-ray heating before shock attenuation [2], the range is appropriate. The fitting constant in Eq. (1) is 0.5 based on Duocel data [8]. If the foam is fabricated to an initial density of 270 kg/m^3, δ = 0.1. Equation (1) with a = 0.5 and σ_{ys} = 195 MPa gives σ_p = 3.1 MPa.

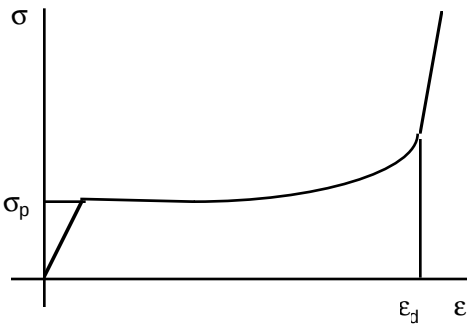

Figure 1: Generic stress strain curve for a foam.

Gibson and Ashby then derive an estimate for the foam thickness required for impact attenuation. Their idea is that the impact loads the foam along the foam's stress strain curve until densification. Integrating the function shown on Fig. 1 until densification gives an energy density absorbed on impact which can then be used to estimate the required foam thickness given the impact energy per unit area. This estimate is appropriate for shipping packaging analysis. Unfortunately this model does not account for shocking the foam which is expected in our case since the nominal incoming peak pressure is nearly three orders of magnitude greater than the plateau stress.

In fact, the shocking of the foam occurs in three distinct phases. In the first phase, kinetic energy in the pressure pulse in ice is absorbed in the foam as kinetic and internal energy. At the same time, a precursor pulse is launched. This phase is over on the order of microseconds . In the next phase, the main pressure pulse decreases as the foam continues to crush. During this phase, the kinetic energy in the crushing converts to internal energy while the precursor continues to advance. This phase is completed on the order of tens of microseconds. In the final phase, the main pulse dissipates leaving only the precursor. If the foam was very thick, we would expect a long square pulse with height σ_p and width τ related by the momentum conserving relation $I_0 = \sigma_p t$, where I_0 is the impulse contained in the original pressure pulse that went through the ice. It is this precursor pulse that loads the object that the ice/foam layer protects. The long time (order hundreds of microseconds) behavior of the protected object due to the loading requires a two dimensional structural response simulation. Here, we just want to estimate the amount of foam needed to sustain the transient crush. To do this estimate, we use the well known snowplow model.

The snowplow model in a foam assumes Rankine-Hugoniot jump conditions across the shock interface and that the shock irreversibly crushes the foam to its solid state. If the density in the unshocked foam is ρ_0 and the unshocked foam is under no pressure and has no material velocity, then the density, material velocity, and pressure in the shocked material is given by

$$\rho = \rho_s \quad (2)$$

$$u = \mu V_s \quad (3)$$

$$P = \rho_0 u^2 / \mu \quad (4)$$

where

$$\mu = 1 - \delta = 1 - \rho_0 / \rho_s \quad (5)$$

is the initial porosity, ρ_s is the solid material density, and V_s is the shock speed.

The shock or foam front s starts at 0 and moves as

$$\frac{ds}{dt} = V_s \quad (6)$$

s is the length of uncrushed foam consumed by the shock. The mass per unit area of shocked material is then ρ_0 s. Therefore, the impulse carried by the main pressure pulse in the crushing foam is

$$I = \rho_0 s u \quad (7)$$

To limit σ_p loading pressure, low density foams with $\delta < 0.2$ are of interest. Because of the low foam density, a tensile wave would be reflected at the ice-foam interface . However, ice can support a tensile wave of only a few bars, so we assume all of the

impulse in the ice is delivered to the foam, or I = I_0 initially. As the main pressure pulse propagates, some of the impulse in the main pressure pulse is lost to the precursor so that Eq. (7) becomes

$$I_0 - \sigma_p t = \rho_0 s u \qquad (8)$$

Note that this equation applies only for t < I_0 / σ_p.

Eliminating V_s in Eq. (3) with Eq. (6) and then substituting the results into Eq. (8) gives an ODE equation for s^2 which when solved with the initial condition s = 0 gives

$$s^2 = (2I_0^2 / \rho_0 \mu \sigma_p)(x - x^2/2) \qquad (9)$$

where the dimensionless quantity

$$x \equiv \sigma_p t / I_0 < 1$$

We now use Eq. (9) to solve Eq. (8) for u^2 as a function of x and substitute the result into Eq. (4) to obtain

$$P = \sigma_p \frac{(1-x)^2}{2x(1-x/2)} \qquad (10)$$

P falls to σ_p when x=1-1/$\sqrt{2}$. Substituting this result into Eq. (9) gives our estimate of the foam crush depth

$$D = \sqrt{I_0^2 / 2\rho_s (1-\delta) a \sigma_{ys} \delta^{5/2}} \qquad (11)$$

where we have substituted Eqs. (1) and (5). We will check our estimate with CALE simulations.

3.0 CALE simulations

CALE is an arbitrary Euler-Lagrange hydrodynamics code with various equation of state and material strength models that can be chosen by the user. Our ice/foam simulations consist of a simple 1-D geometry with 1mm of ice covering 2 cm of aluminum foam. The left boundary condition is a pressure pulse with peak pressure of 2 GPa and an impulse of 220 Pa-sec. The right boundary condition is a rigid wall.

The ice is treated as a hydrodynamic solid with a Gruneisen equation of state with reference density 917 kg/m^3, an attainable minimum pressure of zero, a sound speed of 3236 m/s and a Gruneisen parameter of 0.6 [10]. The ice is not allowed to support tensile waves, forcing the entire pressure pulse into the foam.

The foam is treated as a porous solid with a Gruneisen equation of state applied to the base material aluminum. To implement this model, CALE requires a crush curve of the form

$$P_c = -P_{c0} \ln(\mu)$$

where the porosity μ varies with the crushing. Converting porosity to strain and compaction pressure P_c into stress, we get a curve similar in appearance to Fig. 1 but without the elastic portion. Ignoring the elastic portion, we have σ = σ_p at the initial porosity μ = 1-δ which yields

$$P_{c0} = -\sigma_p / \ln(1-\delta)$$

for use in CALE.

We ran simulations with foam density ratios of 0.1, 0.15, and 0.2 for impulses of both 220 and 440 Pa-sec. The doubled impulse runs were meant to model the effect of debris impulse in addition to cold x-ray impulse. Figures 2 and 3 show the foam front and energy deposition histories for the 220 Pa-sec, 0.1 foam density ratio simulation.

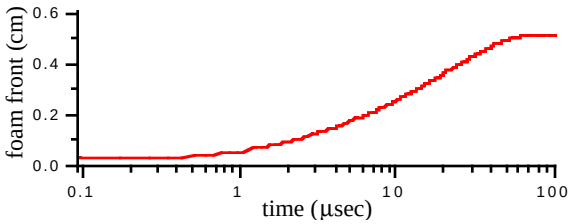

Figure 2: Foam front history for an initial foam density ratio of 0.1 and an impulse of 220 Pa-sec (2.2 ktap).

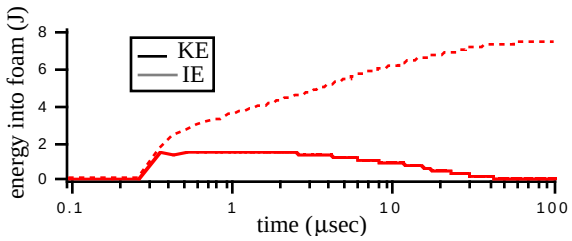

Figure 3: Foam energy deposition history for an initial foam density of 0.1 and an impulse of 220 Pa-sec.

Note that total deposition of about 6 J of kinetic energy from the ice into kinetic and internal energy in the foam is over in about 4 μsec with almost half of the deposition occurring less than 1 μsec. Over this 4 μsec period, the pressure has already dropped from 2.0 GPa (20 kbar) to 10 MPa (100 bar). Comparing Fig. 3 and 2, we see that the ice kinetic energy is absorbed by the time the foam has squeezed down by about a millimeter. As the kinetic energy is converting into internal energy and the main pressure pulse dissipates, the foam has squeezed down by 0.516 cm. These results are only slightly modified with better numerical resolution.

With the presence of heat in the foam, we checked if the foam can melt. We must first consider the amount

of energy deposition from 14 MeV neutrons and hot (11 keV BB) x rays before the shock arrives. The fluence of these radiations due to a 20 MJ capsule 10 cm away are 12 kJ/cm^2 and 100 J/cm^2 respectively [2]. Monte Carlo calculations show that the neutrons deposit 42.6 J/g nearly uniformly into the foam. Aluminum opacities integrated over an 11 keV BB show that the hot x-rays deposit 500 J/g into the first tenth of a millimeter of the foam. Although this is not hot enough to melt given the initial aluminum temperature, the material properties of the foam walls will be severely weakened. At 1 mm, the hot x-ray deposition drops to 160 J/g. At this point, the aluminum temperature rises to around 76.3C assuming a cryo start off temperature of -150 C and using a heat capacity of 0.897 J/g-K [9]. Further in, the hot x-ray deposition becomes less severe. Thus, before the shock arrives, 1mm of foam is rendered useless because the yield strength of the foam walls has dropped significantly due to the heating. (This should be contrasted to polymer foams whose performance is degraded over its entire length due to neutron deposition [2].) It is not clear what this weak foam layer does to shock transition from ice into foam and has not been modeled in our CALE simulations. If we assume that the shock travels unmolested into the foam beyond 1mm, then we can proceed with our estimate because beyond this point, the foam material characteristics are nominal.

The highest per gram internal energy density was found for the case of 440 Pa-sec impulse on a 0.1 density foam. For this case, a maximum of 553 J/g was deposited in a thin layer of fully crushed foam that travels with the crush front. If we add 42.6 J/g for deposition from the neutrons and a maximum additional 160 J/g from the hot x-rays, we have deposited a total of almost 760 J/g. The foam starts at -150 C. Aluminum melts at 660 C with a latent heat of melting of 397 J/g. Therefore, we need 727 J/g to melt and 397 J/g through melt. Thus we are at melting but there is not enough deposition to get over the latent heat. A foam with a higher density ratio suffers less from crush heating and as we will see, squeezes down less requiring less initial thickness.

We compare Eq. (11) with the results from the CALE simulations on Fig. 4:

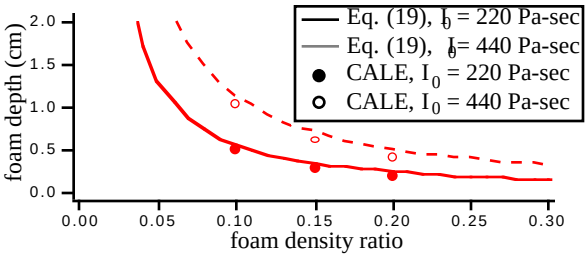

Figure 4: Foam depth vs. foam density ratio for Al 6101-T6 based foam. Al 6101-T6 has a density of 2700 kg/m^3 and a yield stress of 195 MPa.

We see good agreement with our estimate and the final amount the foam has squeezed in the CALE simulation. The predicted time at which foam stops crushing is smaller than what CALE predicts. With $x=1-1/\sqrt{2}$, $t = 0.293\ I_0\ /\ \sigma_p$, but from Figs. 2 and 3, $t = I_0\ /\ \sigma_p$ appears to be a more realistic stop time. Such inaccuracies are expected given the relative simplicity of the snowplow model.

We now make some comparisons to frost mitigation which is an alternative protection scheme in which the frost is both the ablator and shock absorber. We again use Eq. (11), replacing σ_p terms (c.f. Eq. (1)) with some minimum pressure P_{min}. For ice frost, $\rho_s = 917$ kg/m^3. For frost density 10% of ice density, δ=0.1. We then calculate the frost depth required to attenuate the 220 Pa-sec impulse down to a $P_{min} = 3.1$ MPa to be 0.973 cm which is almost twice the depth the aluminum foam for the same performance. Equation (11) can also be used to quickly estimate foam crush depths for other metal foams.

Equation (11) and the CALE simulations show less foam is needed if a higher foam density is selected. Also, foam heating is less severe. However, Fig. 5, calculated from Eq. (4), shows the increased precursor pressure, i.e. protected object loading pressure, obtained when higher foam densities are used. Therefore, the designer must balance the space allotted for the foam with how much loading the protected object can withstand.

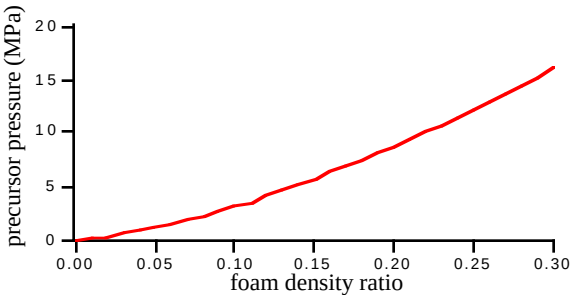

Figure 5: Precursor pressure for the foam of Fig. 4. Since this quantity is used to load CALE's foam equation of state crush curve, the simulation precursor pressures agree identically.

To demonstrate the precursor pressure loading, we consider the static stress of a simply supported circular plate, e.g. a can lid. The peak stress due to a loading pressure is [11]:

$$\sigma = 1.24 P_L \left(\frac{R}{d} \right)^2$$

where R is the lid radius, d is the lid thickness and P_L is the loading pressure. Assuming the shock from the foam is completely reflected at the foam/lid interface, we have $P_L = 2\ \sigma_p$. For 10% foam, $\sigma_p = 3.1$ MPa. For a 304 stainless steel can, $\sigma_y = 240$ MPa [12]. If the can cross sectional area is 1 cm^2, d > 1 mm, to keep the peak static stress below the yield stress.

The reflected shock may lead to spall at the foam edge that was crushed. To check if this will indeed occur, we will need to know the tensile limit for spall of the crushed foam with the caveat the foam is simultaneously heated If the tensile limit for spall is the yield strength of solid aluminum, then spall is a strong possibility because order 1-2 mm of foam has been heated by crushing and hot x-rays and the heating greatly reduces the yield strength. On the other hand, heating makes the aluminum more ductile which increases the plastic strain to failure so that even if the tensile limit for spall, reduced by heating, is reached, the material may not fail.

4.0 DYNA simulations

For the preliminary design phase of this work, we use DYNA. DYNA is a finite element continuum mechanics code and can deal with realistic shapes more easily than most finite difference hydrocodes In addition, the DYNA material types and equations of state are more versatile than those of CALE.

We ran an axisymmetric DYNA calculation on the assembly shown on Fig. 6. The 10% of solid density Duocel foam block is cylindrical with an embedded spherical shell 304 stainless steel sample case. We chose a shell width of 2 mm based on our lid radius estimates of Section 3. The entire assembly is free to move in any direction and is loaded uniformly at the bottom with a triangular pressure pulse in time such that the peak is 2.0 GPa (20 kbar) and the impulse is 220 Pa-sec (2.2 ktap) to model the recoil impulse from cold x-ray deposition. The basic zoning is roughly two elements per radial millimeter. The zoning in the foam over half of the bottom foam layer is finer towards the pressurized surface. This foam shock entry piece is indicated by the horizontal line between the can and the loading plane. The ratio of thickest to thinnest zone is a factor of six. This was done to avoid an immediate numerical instability at the pressurized surface.

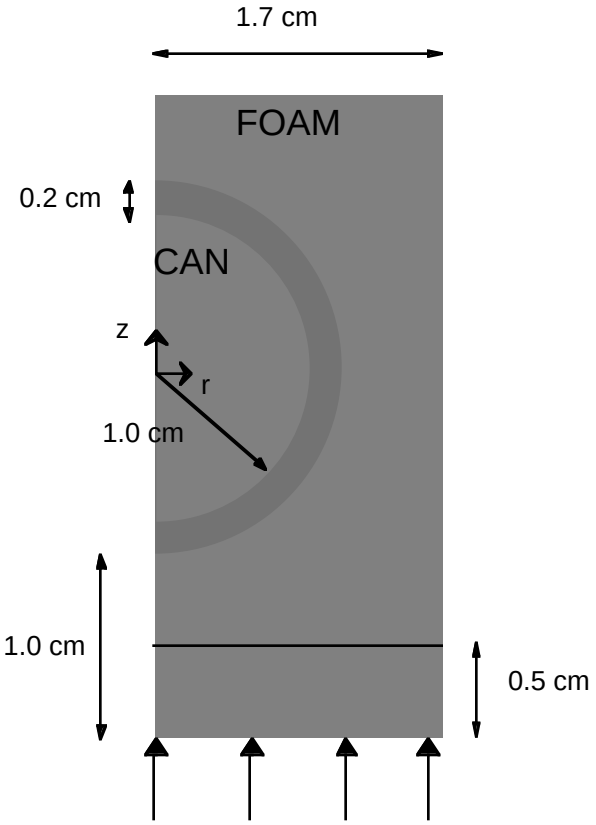

Figure 6: Schematic of DYNA simulation geometry. The large arrows indicate the loading. The horizontal line near the bottom of the foam indicates the break in axial zoning. Below the line, in the foam shock entry piece, the zoning is finer towards the loading.

Beyond 10 μsec, a slowly growing rigid body z velocity becomes noticeable. Since the transient pressure pulse is concluded at 10 μsec, we remesh at this time to control the slower numerical instability. The meshing is similar to that used to start the problem but no ratioed zoning is required.

The steel was modeled as an elastic perfectly plastic material with density 7900 kg/m^3, Young's modulus 210 GPa, Poisson ratio 0.31, and yield stress 240 MPa [12]. Hardening and failure beyond yield was not specifically modeled. However, failure in 304 stainless steel occurs when the effective plastic strain reaches 0.4 [13].

The Duocel foam was modeled with a more detailed crush curve than used in Section 3. The curve stays along the plateau stress until densification starts. Then a curve fit through densification up to the fully densified regime is used. In the fully densified regime, there is a linear stress-strain behavior with the slope equal to the Young's modulus of aluminum which is 69 GPa [9].

The DYNA foam model also requires the shear and bulk unloading moduli. The moduli vary depending on

the crush condition of the foam, but the DYNA model accepts only one value for these quantities. Since most of the foam is exposed only to the precursor pressure and is thus not strongly crushed, we take the uncrushed value for the shear modulus. For 10 % foam, the shear modulus is 345 MPa [8]. Assuming unloading is most important in the strongly crushed foam edge and that the incoming pressures nearly solidify the foam, we take the as the unloading modulus the bulk modulus of solid aluminum which is 74 GPa [9].

The DYNA foam model also requires a foam yield stress and a foam tensile limit. For uniaxial loading which is essentially what we have here, the foam yield stress is just the plateau stress defined in Eq. (4), although a non-trivial correction for multiaxial loading is available [14]. The tensile limit is taken to be the foam yield stress, negative in tension, since tension beyond this point will make the stretching foam walls touch. Further tension up to the solid aluminum yield stress would lead to spall.

The entire foam model uses nominal solid material parameters. This idea breaks down at the foam edge where crushing and hot x-ray heating lead to near melt conditions. Since the edge is thin, we suspect that such effects do not play a large part in the global material response. However, to model spall properly, these thermal effects must be calculated self-consistently. This would require an elastic-plastic hydrodynamic foam model with strain and temperature dependent yield, yield hardening, compaction, unloading, and shear. Both CALE and DYNA have pieces of this model, but major code development would be required to fully assemble such a model.

The results of our simulation are shown in Fig. 7. The effective stress at 130 μsec has a maximum of 22 MPa which is an order of magnitude below the stainless steel yield stress of 240 MPa. For time out to 400 μsec, the maximum effective stress drops. Given the order km/sec shock speeds and

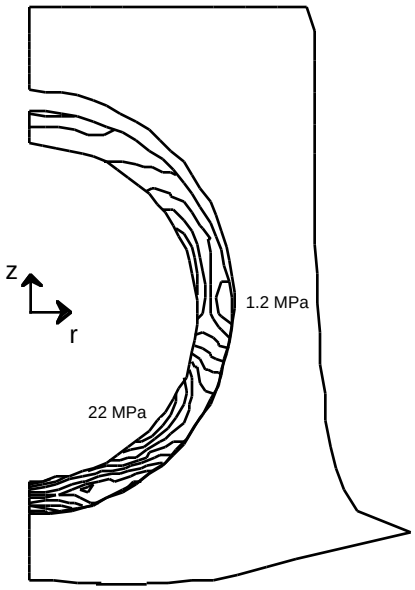

Figure 7: Nine evenly space contours of Von Mises effective stress from the indicated minimum 1.2 MPa and maximum 22 MPa at 130 microseconds. The outline of the crushed foam is also shown.

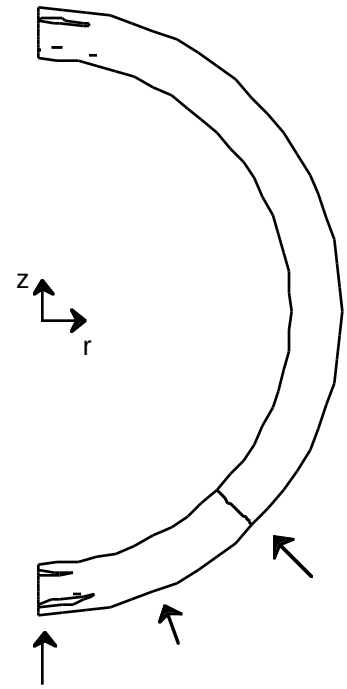

Figure 8: Outline of bare can DYNA simulation. The arrows at the bottom of the can indicate the load surface. Inside the small contours at the poles of the can, the effective plastic strain has exceeded the failure point. The contours were taken 160 microseconds after the initial loading.

the order cm dimensions of the problem, 100 or so microseconds should be long enough to resolve wave bouncing.

The DYNA simulations give qualitatively similar results to the CALE simulations. Plateau pressure precursors are launched and the main pressure pulse decays away in under 10 μsec. The kinetic energy pulses up and then decays down over tens of μsec as the front of the foam crushes from 1 cm thick to about 0.4 cm thick. Finally, the DYNA rigid body z velocity is consistent with the incoming momentum (impulse x radial surface load area) and assembly mass until the previously mentioned slow growth instability becomes noticeable.

We compare our results to the bare can simulation shown in Fig. 8. This simulation is initialized with a 220 Pa-sec, 0.2 GPa pressure pulse. The gentler pulse is used here because the 2 GPa initialization is violently unstable to various zonings attempted. The simulation ran out to several 100 μsec without changes in kinetic energy and rigid body z velocity beyond the initial pulse. The z velocity is consistent with the incoming momentum (impulse x spherical surface load area) and can mass. The zoning that achieved this required 20 elements over the 2 mm shell with a reduction in zone size by a factor of five from the inner to the outer element. Despite the gentler loading, the unprotected can reaches the failure point at 160 μsec.

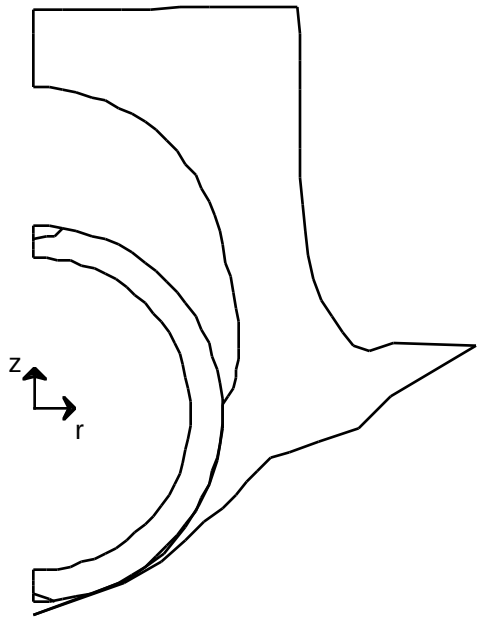

Figure 9: Doubled impulse simulation. Inside the small contours at the poles of the can, the effective plastic strain has exceeded 0.005 with the maximum value of 0.014. Also pictured is the outline of the crushed foam. The contours were taken 350 microseconds after the initial loading.

Finally, we ran a sample case assembly problem identical to Fig. 7 except the impulse was doubled to 440 Pa-sec (4.4 ktap) to approximately account for the additional impulse due to plasma debris loading. The effective plastic strain at 350 μsec is shown in Fig. 9. Note the greater deformation of the foam then for the 220 Pa-sec impulse. For this load, the can does yield, but the plastic strain accumulated does not go above 0.014 which is a order of magnitude below the 0.4 effective plastic strain to failure in 304 stainless steel.

5.0 Future work

We have demonstrated that it is possible to protect a radiation sample case from plastic failure due to cold x-ray ablation and plasma debris shocks with a reasonable amount of foam. An immediate task is to vary peak pressures and impulses in the DYNA simulation to see how far we can push the protection scheme. Future tasks also include scoping out of better materials and experimental verification of existing calculations. Eventually, the calculations will be extended by modeling ablating x-rays and heating radiation coming into the sides as well as the bottom, can fasteners, and shrapnel, requiring a three dimensional model with material penetration.

A critical problem is the possible melt and/or spall of the foam. Melted foam can drop to the chamber floor

and spall can make nasty projectiles. Higher aluminum foam density leads to less heat on crushing, but even without crushing, hot (11 keV BB) x-ray deposition leads to a significant reduction in yield strength on the front foam layer. This may not hurt the performance of the remainder of the foam, but can lead to spall when reflected waves impinge back onto the layer. A solution to this problem may be found by using a foam based on a metal whose radiation absorption heating, crush heating, and heat capacity lead to a temperature rise that not only keeps the metal below its melting temperature but also below a temperature where the yield strength drops significantly. An alternative foam material may also be required so that radioactive decay from neutron activation drops to a prescribed level in the shortest possible time.

It has recently been found that a B_4C ablator is easier to use than ice and additional target chamber contamination for a 3 cm diameter is less than a third of the unavoidable contamination due to the 20 MJ target itself. Calculations of the cold x-ray impulse through this ablator and propagation of hot x-rays on into the foam will have to be done.

The one dimensional model, Eq. (11) corroborated with CALE simulations, has been used to help estimate the space required for NIF target chamber protection mechanisms. Experimental validation of the one dimensional model should therefore be done as soon as possible. This can be accomplished by shooting ice/foam layers of varying foam densities with varying impulses. The impulse, final foam length and pressure delivered to the back of the foam may be measured to check the validity of our calculations. Two possibilities for shooting are using NOVA to ablate plastic and send a NIF comparable pressure pulse into the foam or to use the gas gun facility to accomplish essentially the same task with a flyer plate. Some more thinking in terms of ease of the experiment, usefulness of the results, and cost must be done before a final choice can be made. An added advantage of a experiment is that spall due to crush heating, reduced yield strength, and reflected waves can be detected and perhaps conclusions can be drawn on its severity.

Acknowledgments

We wish to thank Douglas Faux of LLNL Mechanical Engineering for helpful advice for using DYNA.

This work was performed under the auspices of the United States Department of Energy by Lawrence Livermore National Laboratory under contract W-7405-ENG-48.

References

1. Kruger, H., Lawrence Livermore National Laboratory, Livermore, CA, NIF Briefing for A. Spero, D Division Leader (1995).

2. DiPeso, G., Farley W.,, Gerassimenko M., Managan, R., Maxon, S., Serduke, F., Simonson. G., Suter, L., Tabak, M., and Tobin, M., *High Power Laser Source Evaluation (U),* Lawrence Livermore National Laboratory, Livermore CA, CD-96-0002-DR-1 (1996).

3. Managan, R., Lawrence Livermore National Laboratory, Livermore, CA, NIF Briefing for A. Spero, D Division Leader (1996).

4. Peterson, P., Lawrence Livermore National Laboratory, Livermore, CA, NIF Chamber Dynamics Meeting (1996).

5. *CALE User's Manual,* contact Robert Tipton, Lawrence Livermore National Laboratory, Livermore, CA.

6. *DYNA2D Manual,* contact Edward Zywicz, contact Robert Tipton, Lawrence Livermore National Laboratory, Livermore, CA

7. Gibson, L. J. , *Cellular Solids: Structure and Properties,* (Pergamon Press, Elmsford NY, 1988). Ashby, M. F., "The Mechanical Properties of Cellular Solids,"M*etallurgical Transactions A,* **14 A,** 1755 (1983).

8. *The Physical Properties of Duocel Reticulated Aluminum Foam*, Energy Research and Generation Inc., internal document..

9. *ASM Metals Handbook 10th Edition, Volume 2 Properties and Selection: Non Ferrous Alloys and Special Purpose Materials.* (ASM International 1990).

10. Hobbs, P. V., *Physics of Ice,* (Clarendon Press, Oxford, 1974).

11. Baumeister, T., *Mark's Standard Handbook for Mechanical Engineers,* (McGraw Hill Book Company, New York, 1978).

12. Anderson, H. L., *A Physicist's Desk Reference,* (American Institute of Physics, New York, 1989).

13. Huang, G. L., Matlock, D. K., Krauss, G., "Martensite Formation, Strain Rate Sensitivity, and Deformation Behavior of Type 304 Stainless Steel Sheet," *Metallurgical Transactions A,* **20**, 1239 (1989).

14. Gibson, L. J., Ashby, M. F., Zhang, J., Triantfillou, T., "Failure Surfaces for Cellular Materials

Under Multiaxial Loading-Modeling," *International Journal of Mechanical Science*, **31** 635 (1985).

Technical Information Department • **Lawrence Livermore National Laboratory**
University of California • Livermore, California 94551